



# Triaxial mechanical behaviour of hybrid basalt–polypropylene fibre-reinforced concrete: The effect of micro-fibres at multi scale levels

Qiang Fu · Mengxin Bu · Li Su · Lei Liu · Lou Chen · Ning Li · Ditao Niu

Received: 6 January 2021 / Accepted: 13 May 2021  
© The Author(s) 2021, corrected publication 2022

**Abstract** The triaxial mechanical properties of hybrid basalt–polypropylene fibre-reinforced concrete (HBPRC) were investigated in detail. The different effects of micro-basalt fibre (BF) and micro-polypropylene fibre (PF) on the triaxial properties of concrete were revealed. The strength criterion for HBPRC was established. The results showed that the hydrostatic behaviour, volumetric strain, peak deviatoric stress, elastic modulus, and Poisson's ratio of HBPRC are affected by not only the confining pressure but also the BF and PF. The confining pressure gradually changes the failure mode of

HBPRC from split failure to shear failure and extrusion plastic flow failure. The BF and PF mainly improve the strength and deformation performance of concrete, respectively. A nonlinear Mohr–Coulomb (M–C) strength criterion for HBPRC, which takes into account the fibre effect, is established. The calculated results performed using the proposed criterion agree well with the experimental results.

**Keywords** Basalt fibre · Polypropylene fibre · Hydrostatic behaviour · Nonlinear M–C strength criterion

---

Q. Fu (✉) · M. Bu · L. Su · D. Niu  
School of Civil Engineering, Xi'an University of  
Architecture and Technology, Xi'an 710055, People's  
Republic of China  
e-mail: fuqiangcsu@163.com

L. Liu  
State Key Laboratory of Water Resources and  
Hydropower Engineering Science, Wuhan University,  
Wuhan 430072, People's Republic of China

L. Chen (✉)  
School of Civil Engineering, Central South University,  
Changsha 410075, People's Republic of China  
e-mail: chen.lou.17@ucl.ac.uk

N. Li (✉)  
School of Civil Engineering, Qingdao University of  
Technology, Qingdao 266033, People's Republic of  
China  
e-mail: lining1989csu@163.com

## 1 Introduction

The addition of fibres can significantly reduce the brittleness of concrete and improve the tensile properties and ductility of concrete [1–8]. In particular, the mixing of rigid fibres and flexible fibres is an ideal mode of fibre addition to improve the tensile properties and ductility of concrete. The high elastic modulus of the rigid fibres and the high ductility of the flexible fibres allow them to play the role of crack bridging in different deformation stages of concrete and significantly improve the strength and deformation performance of concrete [9]. Basalt fibre (BF) is eco-friendly and high-performance inorganic micro-fibre with the diameter of 10–20  $\mu\text{m}$ . BF is made by melting and drawing basalt ore at a high temperature, and the



production process has low energy consumption. BF has good mechanical properties, with an elastic modulus of 93–115 GPa and a tensile strength of 200–5000 MPa. Additionally, BF has good temperature stability and chemical stability [10, 11]. Polypropylene fibre (PF) is a flexible micro-fibre with the diameter of 15–45  $\mu\text{m}$  and low elastic modulus but good ductility and chemical inertness; thus, it can stably exist in the alkaline environment of concrete [12, 13]. Therefore, when micro-BF and micro-PF are mixed into concrete, their crack bridging effect and hybridity effect can restrain the crack propagation in the concrete, reduce the brittleness of concrete, and improve the ductility of concrete.

At present, there are limited research results on the mechanical properties of hybrid basalt–polypropylene fibre-reinforced concrete (HBPRC) but abundant research results on the mechanical properties of concrete reinforced with BF or PF alone. Studies have indicated that at the appropriate content, BF or PF can significantly improve the tensile, flexural, and deformation properties of concrete, but their improvement effect on the compressive strength of concrete is limited. The addition of mineral admixtures can improve the dispersion of BF or PF and the bonding properties between BF or PF and the concrete matrix, enhancing the positive effects of the BF or PF on the mechanical properties of concrete [14–25]. Regarding the mechanical properties of HBPRC, the results of Li et al. [26], Smarzewskietal et al. [27], and Wangetal et al. [28] indicate that at the appropriate content, hybrid BF and PF have a relatively significant improvement effect on the flexural strength and splitting strength of concrete, but their improvement effect on the compressive strength of concrete is relatively limited, and the improvement effect of hybrid BF and PF on the mechanical properties of concrete is greater than that of BF or PF alone. Zhang et al. [29] and Fu et al. [30] found that, at the appropriate content, hybrid BF and macro-PF or micro-PF improved not only the static compressive strength of concrete but also the impact resistance, respectively. However, the aforementioned research results on the mechanical properties of HBPRC have two problems. First, owing to the differences in the performance of the concrete matrix, there is no universal agreement on the appropriate content of hybrid BF and PF or the appropriate proportions of BF and PF. Second, studies on the mechanical properties

of HBPRC have focused on uniaxial loading, research results for the mechanical properties of HBPRC under triaxial loading are lacking. However, concrete in actual applications is normally in triaxial stress state. The concrete in concrete filled steel tube, building nodes, the prestressed concrete anchorage areas, and the nuclear reaction pressure vessel is typical example. The triaxial stress-deformation behaviour contains comprehensive mechanical information regarding the concrete, which is more helpful for the accurate design and analysis of concrete structures. Therefore, to fully understand the mechanical properties of HBPRC and promote its application, the triaxial mechanical properties of HBPRC must be investigated.

Research on the triaxial mechanical properties of concrete began in 1929 [31]. Subsequently, many scholars have comprehensively studied the triaxial mechanical properties of ordinary concrete, high-strength and high-performance concrete, fibre-reinforced concrete, and lightweight aggregate concrete. The strength and deformation properties of concrete are enhanced with an increase in the confining pressure. With the increasing confining pressure, the increase range of the peak stress of concrete gradually decreases, and the post-peak stress–strain curve gradually transforms from strain softening to strain hardening. The failure mode of concrete gradually changes from longitudinal split failure to oblique shear failure and transverse expansion failure with multi-cracks. The addition of fibres can significantly improve the triaxial deformation performance of concrete and reduce the damage degree of concrete. With an increase in the axial pressure, the volume deformation of concrete gradually changes from volume contraction to volume expansion. With the increasing confining pressure, the volume contraction deformation of concrete increases, and the volume expansion deformation decreases [32–45]. Malecot et al. [46], Zingg et al. [47], Vu et al. [48], and Piotrowska et al. [49] systematically studied the triaxial mechanical properties of concrete materials under high confining pressures ( $\geq 600$  MPa). Their results indicated that under a high confining pressure, concrete is similar to a non-cohesive granular stacking, and the concrete performance is mainly affected by the compacted cement matrix; under a low confining pressure, the pore structure significantly affects the triaxial mechanical properties. In addition, according to the relationship between the volume deformation and the evolution of



the pore structure, it is concluded that because of the more regular shape and difficult compaction of air pores compared with the capillary pores, capillary pores are compacted, followed by the air pores [46, 47].

The strength criterion of concrete is often used to determine the strength of concrete in a given stress field and the range of the plastic zone at the failure of concrete, which plays an important role in the rational design of concrete structures. A variety of failure criteria for concrete materials based on mechanical theory or empirical analysis have been proposed, such as the Mohr–Coulomb (M–C) strength criterion, Hook–Brown strength criterion, Drucker–Prager strength criterion, octahedral strength criterion, and power-law strength criterion. These strength criteria can be used to determine the strength variation law of concrete in a complex environment and the complex stress state or the range of the plastic zone at failure and to ensure the rational design of concrete structures [34, 50–55]. However, the aforementioned strength criteria may be applicable only to specific types of concrete materials, and their parameters may differ for different types of concrete materials. Therefore, a reasonable strength criterion for HBPRC should be established on the basis of triaxial tests, to provide reasonable theoretical support for the design of HBPRC structures.

In this study, the triaxial mechanical properties of HBPRC in the confining pressure range of 0–20 MPa were investigated, and the effects of BF, PF, and the confining pressure on the hydrostatic behaviour, deviator behaviour, and limit state of HBPRC were analysed. The mechanism whereby the BF and PF affected the triaxial mechanical properties of HBPRC was analysed. Finally, a strength criterion for HBPRC related to the fibre content was established.

## 2 Materials and experimental framework

### 2.1 Materials and mix proportions

The components of the HBPRC mixture included P.O 42.5R ordinary Portland cement (C), silica fume (SF), fly ash (FA), slag powder (SP), fine aggregate (S), coarse aggregate (CA), potable tap water (W), polycarboxylate high-performance superplasticiser (PBS) with a water reduction rate of 30%, BF, and PF. The

chemical composition and physical properties of the C, SF, FA, and SP can be founded in Niu et al. [4]. The CA was mechanically crushed limestone gravel, and the S was river sand. The maximum particle size and apparent density of the CA were 20 mm and 2.7 g/cm<sup>3</sup>, respectively, and those of the S were 4.75 mm and 2.61 g/cm<sup>3</sup>, respectively. The fineness modulus of the S was 2.8. The length, diameter, density, tensile strength, elastic modulus of BF were 18 mm, 15 µm, 2.56 g/cm<sup>3</sup>, 4500 MPa, and 75,000 MPa, respectively, and the corresponding indices of PF were 19 mm, 30 µm, 0.91 g/cm<sup>3</sup>, 270 MPa, and 3000 MPa, respectively.

The reference matrix strength grade of HBPRC was C30. To comparatively study the effects of BF alone, PF alone, and the BF/PF hybrid (as well as the hybrid fibre content) on the triaxial mechanical properties of concrete, a total of five mix proportions were designed in this study, as shown in Table 1. NC, BC, PC, and BPC represent the reference group concrete, single BF-reinforced concrete, single PF-reinforced concrete, and hybrid BF and PF-reinforced concrete, respectively. When hybrid fibres were added, the BF and PF contents were equal. The numeral after the letters (NC, BC, PC, or BPC) represents the fibre volume content (vol.%). For example, BPC-0.1 represents HBPRC with a hybrid fibre content of 0.1 vol.%.

### 2.2 Specimen preparation

The mixing process for the HBPRC was presented by Fu et al. [56]. After the mixing, the uniform mixture was poured into a 100 mm × 100 mm × 100 mm cube mould prepared in advance and compacted on a vibrating table. Then, the specimen together with the mould was placed in a standard curing room with a temperature of 20 ± 2 °C and a relative humidity of > 95%. After 24 h, the specimens were demoulded and kept in the curing room for 28 d. Then, the triaxial mechanical properties of the HBPRC were evaluated via tests. After the specimens were cured for 20 d, their non-formed surfaces were polished by a double-end surface smoothing machine to ensure that these surfaces were smooth and parallel to the opposite surfaces.

**Table 1** Mix proportions of concrete ( $\text{kg}/\text{m}^3$ )

Mixture	BF	PF	C	W	SF	FA	SP	S	CA	PBS
NC	0	0	234.2	161	22	73.2	36.6	683	1162.9	3.66
BC-0.1	2.56	0								
PC-0.1	0	0.91								
BPC-0.1	1.28	0.455								
BPC-0.2	2.56	0.91								

### 2.3 Triaxial compressive test

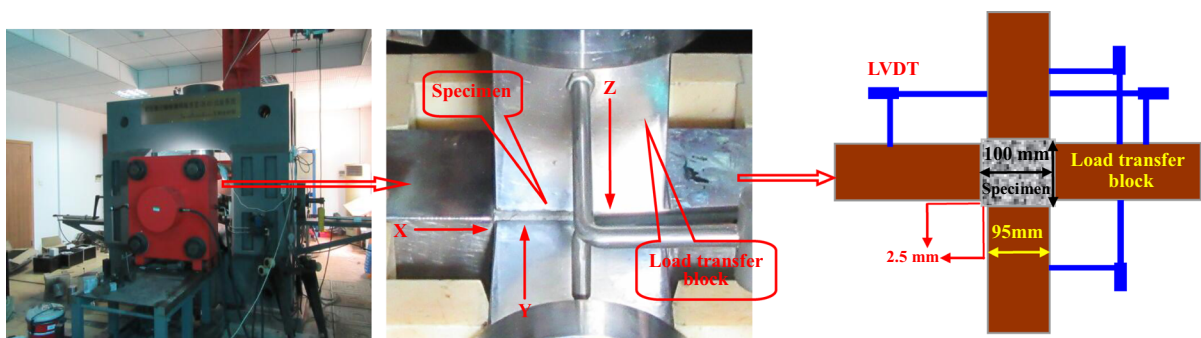
A true triaxial hydraulic servo-controlled test system was used to conduct triaxial compression tests of the HBPRC. The system comprised a servo-controller system, measurement sensors, and a data-acquisition system. Its structure is shown in Fig. 1. The loads in the three principal stress directions were applied by the hydraulic pistons. The maximum longitudinal and lateral load limits for the system were 3000, 2000, and 2000 kN, respectively. The load transfer block had a side length of 95 mm; it was 5 mm smaller than the specimen, to prevent the adjacent load transfer blocks from colliding when the specimen underwent large deformation during the loading process.

Before the loading, a thin layer of lubricating oil was sprinkled onto the surface of the specimen to eliminate the friction between the load transfer block and the specimen. Then, the hydrostatic pressure was increased to the preset confining pressure level along the three principal stress directions of the specimen by the hydraulic pistons with a loading rate of 0.1 MPa/s. While the confining pressure was kept constant, the specimen was loaded to failure at a longitudinal loading rate of 0.1 mm/min. The load datum was collected automatically by the data-acquisition system. The deformation of the specimen was measured

by linear variable displacement transducers (LVDT). To ensure the validity of the experimental results, five specimens of each mix proportion were tested at each loading. The experimental result with large dispersion was deleted, and the average value of other experimental results was taken as the obtained triaxial compressive experimental results of HBPRC.

### 2.4 Microscopic test

To investigate the failure morphologies of the BF and PF after the triaxial test, HBPRC fragments were examined using a Zeiss Gemini SEM 500 field-emission scanning electron microscope. After the triaxial test, HBPRC fragments with a diameter of approximately 5 mm (containing BF and PF) were collected and pasted on a copper plate with a double-sided conductive adhesive. After gold was sprayed onto the fragments, the failure morphologies of the BF and PF were observed at different magnifications.

**Fig. 1** True tri-axial hydraulic servo-controlled test system

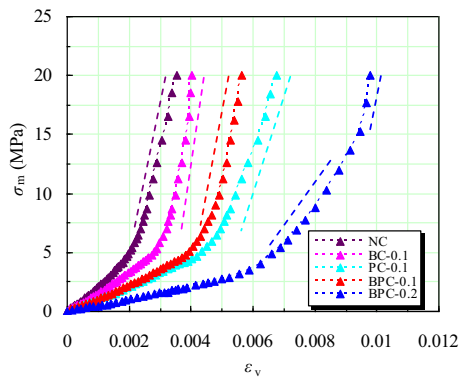


**Fig. 2** Hydrostatic behaviour for HBPRC

### 3 Results and analysis

#### 3.1 Hydrostatic behaviour

Figure 2 shows the relationship between the average stress and the volume deformation of HBPRC during the hydrostatic pressure stage with a maximum confining pressure of 20 MPa.  $\sigma_m = (\sigma_1 + \sigma_2 + \sigma_3)/3$ ;  $\varepsilon_v = (\varepsilon_1 + \varepsilon_2 + \varepsilon_3)/3$ ;  $\sigma_1$  represents the maximum principal stress, i.e. the longitudinal stress;  $\sigma_2$  and  $\sigma_3$  represent the confining pressures; and  $\varepsilon_1$ ,  $\varepsilon_2$ , and  $\varepsilon_3$  represent the strains in the directions of  $\sigma_1$ ,  $\sigma_2$ , and  $\sigma_3$ , respectively. The  $\sigma_m$ - $\varepsilon_v$  curves of NC, BC-0.1, PC-0.1, and BPC-0.1 exhibit a two-stage change trend, whereas the  $\sigma_m$ - $\varepsilon_v$  curve of BPC-0.2 clearly exhibit a three-stage change trend. As shown in Fig. 2, the discontinuous trend lines with the same colour as the  $\sigma_m$ - $\varepsilon_v$  curves of NC, BC-0.1, PC-0.1, and BPC-0.1 represent the variation slopes of the second stages of the corresponding  $\sigma_m$ - $\varepsilon_v$  curves, and the discontinuous trend lines with the same colour as the  $\sigma_m$ - $\varepsilon_v$  curve of BPC-0.2 represent the variation slopes of the second and third stages of the corresponding  $\sigma_m$ - $\varepsilon_v$  curve, respectively. With the addition of the fibres, the maximum strain and the transformation strain between the first and second stages of the  $\sigma_m$ - $\varepsilon_v$  curve increase. This may be because the addition of fibres increases the interface between the fibres and the concrete matrix and introduces air bubbles during the mixing process. In particular, for BPC-0.2, the excessive fibre content not only reduces the dispersion uniformity of fibres but also introduces more bubbles during the stirring process, significantly increasing the transition

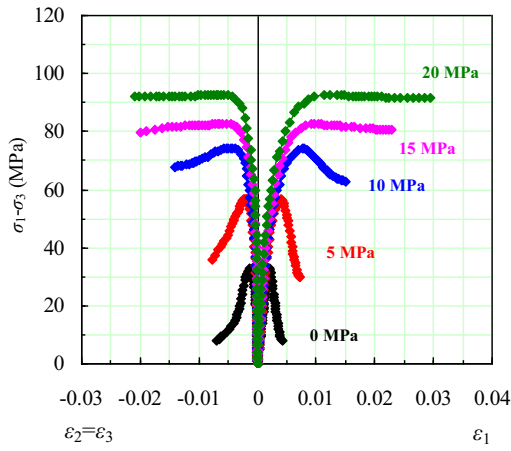
strain between the first and second stages of the  $\sigma_m$ - $\varepsilon_v$  curve.

As shown in Fig. 2, the transformation stress between the first and second stages of the  $\sigma_m$ - $\varepsilon_v$  curve is in the following order: BC-0.1 > BPC-0.1 > PC-0.1 > NC > BPC-0.2, which is identical to the uniaxial strength order of HBPRC (Sect. 3.3). The slope of the second stage of the  $\sigma_m$ - $\varepsilon_v$  curve is in the following order: BC-0.1 > BPC-0.1 > NC > PC-0.1 > BPC-0.2, which is similar to the elastic-modulus order of HBPRC (Sect. 3.3). When  $\sigma_m$  is approximately 15 MPa, the  $\sigma_m$ - $\varepsilon_v$  curve of BPC-0.2 enters the third stage, and the slope in this stage is similar to that in the second stage of the  $\sigma_m$ - $\varepsilon_v$  curve for BPC-0.1. The deformation in the first stage of the  $\sigma_m$ - $\varepsilon_v$  curve is mainly due to the closure of large macrodefects in the concrete under the hydrostatic stress, and the slope of the second stage is mainly affected by the microscopic defects in the concrete as well as the synergistic effects of the fibres and the concrete matrix. For BPC-0.2, the deformation in the first and second stages of the  $\sigma_m$ - $\varepsilon_v$  curve is mainly due to the closure of the many large air bubbles introduced by the poor dispersion of fibres during the mixing process and the secondary macrodefects similar to the major ones of other concrete and introduced by the fibre stacking, respectively, and the slope of the third stage of the  $\sigma_m$ - $\varepsilon_v$  curve is mainly affected by the microscopic defects as well as the synergistic effects of the fibres and the concrete matrix. By comparison, it can be found that BPC-0.2 has more obvious hydrostatic pressure sensitivity.

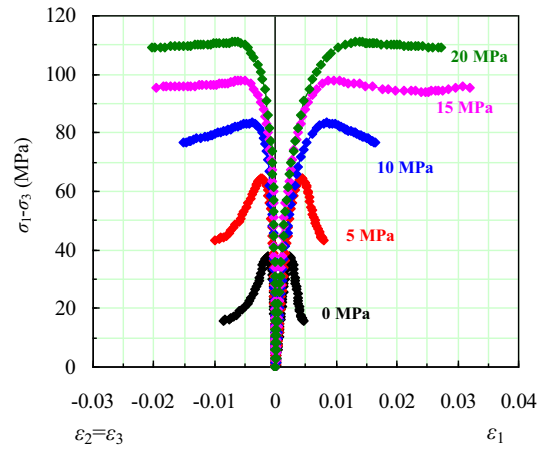
#### 3.2 Deviatoric behaviour

##### 3.2.1 Triaxial stress–strain curves

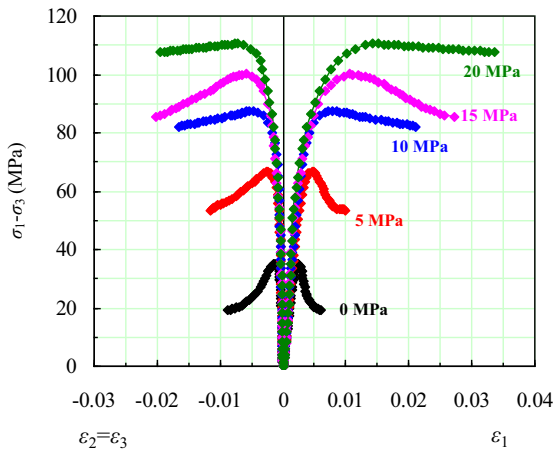
Figure 3 shows the triaxial stress–strain curves of the HBPRC under different confining pressures.  $\sigma_1$ - $\sigma_3$  represents the deviatoric stress of HBPRC, and the strains  $\varepsilon_1$ ,  $\varepsilon_2$  and  $\varepsilon_3$  refer to the ones of HBPRC when the longitudinal load is increased while the confining pressure is constant, excluding the ones formed in the hydrostatic pressure stage. The triaxial stress–strain curves of HBPRC with different mix proportions under different confining pressures exhibit similar changes. With an increase in the confining pressure, the peak stress, the strain corresponding to the peak stress, and the slope of the linear elastic deformation stage of the triaxial stress–strain curve increase, and



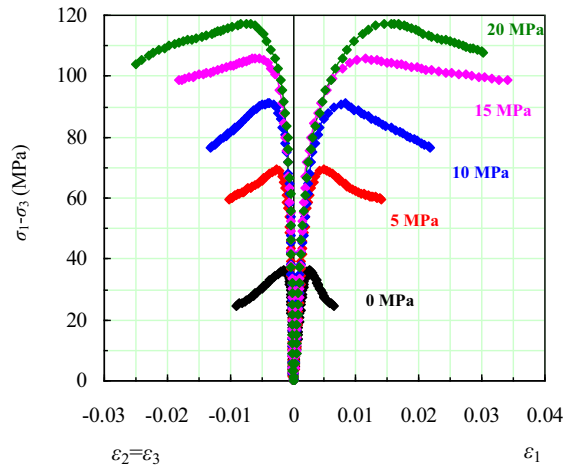
(a) NC



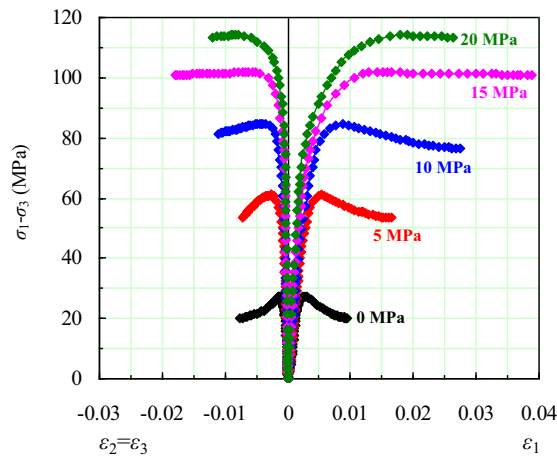
(b) BC-0.1



(c) PC-0.1



(d) BPC-0.1



(e) BPC-0.2





◀ **Fig. 3** Triaxial stress–strain curves of HBPRC at different confining pressures

the ductile deformation characteristics of HBPRC becomes increasingly prominent. However, under the same increase amplitude of the confining pressure, the increase amplitude of the peak stress decreases with the increasing confining pressure. Confining pressure is similar to prestress, which provides interstitial pressure [57] and optimises the internal structural of the HBPRC, inhibits the propagation of cracks in the HBPRC and improves the strength of HBPRC. Additionally, the restraining effect of the confining pressure on cracks results in a HBPRC failure mode with multiple fine cracks (Sect. 3.3.2) rather than a single macrocrack, improving the deformation performance and ductility of HBPRC.

Compared with NC, under no confining pressure and the lower confining pressure, the addition of BF and PF improves the deformability and ductility of concrete. The bridging effect of BF and PF can not only effectively reduce the interpenetration of cracks in HBPRC, but also when some cracks in HBPRC are penetrated, unbroken BF and PF can still inhibit the propagation speed of the penetrated cracks in HBPRC, improving the deformation performance of concrete, reducing its brittleness, and improving its ductility. Compared with the BF, the improvement effect of the PF on the deformation performance and ductility of concrete is more significant. Compared with BF alone or PF alone, the improvement effect of the BF/PF hybrid on the deformation performance and ductility of concrete is more obvious, as shown in Figs. 4a and b. Figure 4c shows the triaxial stress–strain curve of HBPRC under a confining pressure of 20 MPa. Under this high confining pressure, compared with NC, the addition of BF and PF only slightly increases the strain corresponding to the peak stress of concrete, while the ductility deformation of the HBPRC does not change significantly. Both the confining pressure and the fibres have a constraint effect on the propagation of cracks in the HBPRC. However, with an increase in the confining pressure, the constraint effect of the confining pressure on the cracks gradually becomes dominant, weakening the effect of fibre addition on the ductile deformation of concrete.

### 3.2.2 Volumetric strain

The relationship between the volumetric strain  $\varepsilon_v$  and the axial strain  $\varepsilon_1$ , as well as the lateral strains  $\varepsilon_2$  and  $\varepsilon_3$ , of HBPRC under different confining pressures is presented in Fig. 5. Here, positive and negative strains indicate contraction and expansion, respectively. For NC, BC-0.1, PC-0.1, and BPC-0.1, in the initial loading stage of the longitudinal load, HBPRC undergoes volume contraction. Under the continuous action of the longitudinal load, the concrete gradually transitions from volume contraction to volume expansion. With an increase in the confining pressure, the volume contraction strain of the concrete increases, while the volume expansion strain decreases. This is attributed to the constraint effect of the confining pressure on the development of internal defects in the concrete, which is consistent with the research results for the changes in the volume strain of slurry-infilled fibre concrete and ordinary concrete with respect to the confining pressure reported by Farnam et al. [35] and Hammoud et al. [36]. Moreover, compared with NC, the addition of BF and PF slightly increases the volume contraction strain of concrete and significantly reduces the volume expansion strain of concrete. The interface between the fibres and the concrete matrix and the low elastic modulus of the PF increase the volume contraction strain of concrete, and the inhibition effect of the fibres on the cracks reduces the volume expansion strain of concrete. Although BC-0.1, PC-0.1, and BPC-0.1 have the same fibre content, the addition of hybrid BF and PF has a greater reduction effect on the volume expansion strain of concrete, indicating the synergistic effects of the BF and PF for crack inhibition.

Under a uniaxial load, the volume strain of BPC-0.2 also changes from volume contraction strain to volume expansion strain with the increasing load, but the volume expansion strain of BPC-0.2 decreases significantly compared with the other concrete. However, under the confining pressure, BPC-0.2 is in the volume contraction state. As shown in Fig. 3e, in the absence of confining pressure, the final longitudinal compression strain of BPC-0.2 is almost the same as the single lateral expansion strain, so the volume expansion strain of BPC-0.2 occurs at this time. Under confining pressure, the longitudinal compression strain of BPC-0.2 is much greater than the single lateral expansion strain when the longitudinal load is

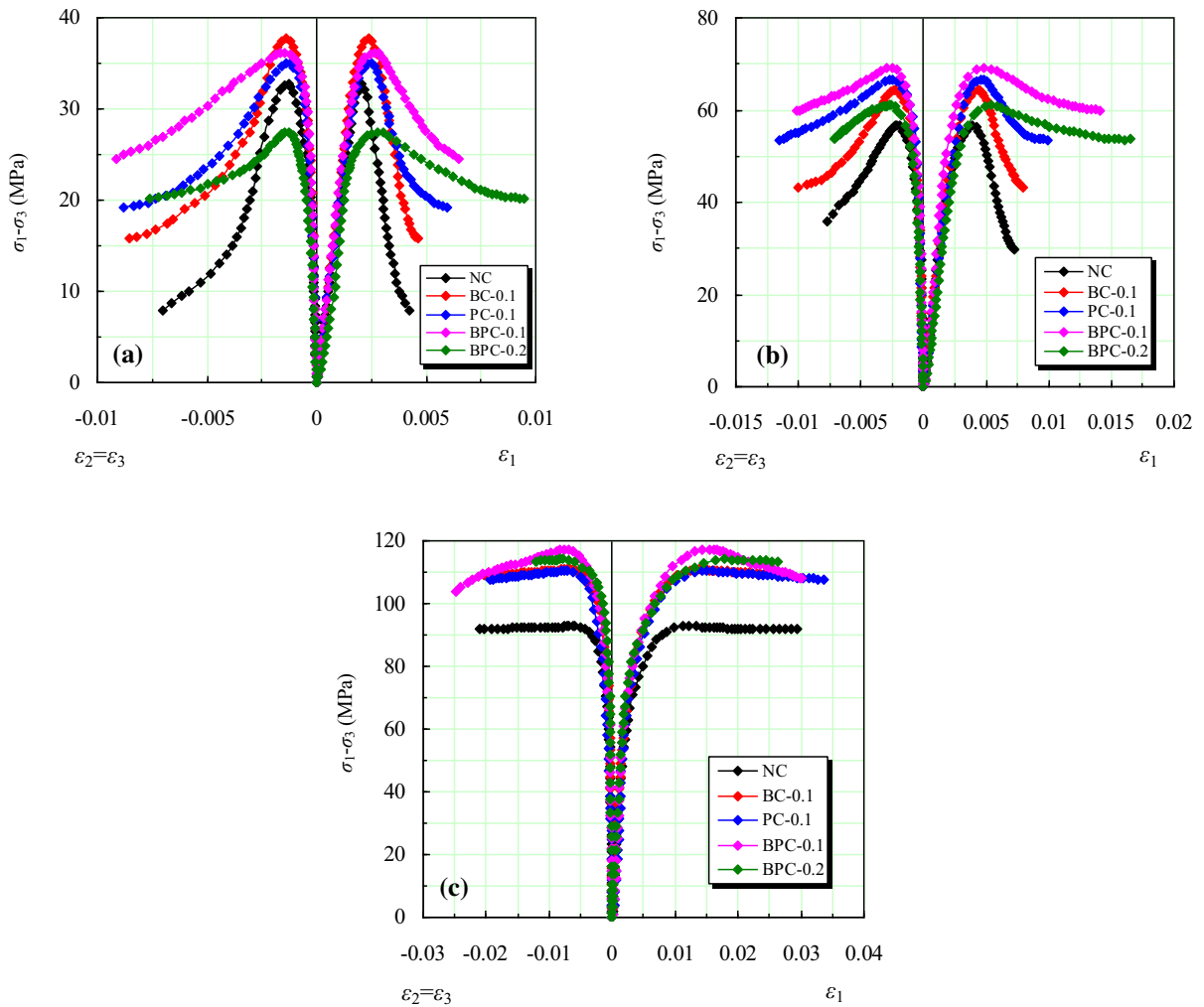


**Fig. 4** Triaxial stress–strain curves of HBPRC at the confining pressure of **a** 0 MPa, **b** 5 MPa and **c** 20 MPa

applied, so BPC-0.2 presents the volume contraction strain. An excessive content of BF and PF reduces the dispersion uniformity of the BF and PF, degrades the bonding performance between the fibres and the concrete matrix, and increases the amount of microscopic defects in the concrete, causing BPC-0.2 to be in the volume contraction state under a longitudinal load. When the confining pressure is high, it reduces the amount of initial defects in BPC-0.2, causing the volume strain of BPC-0.2 to change towards volume expansion, but the change trend is not obvious.

### 3.3 Limit states

#### 3.3.1 Peak deviatoric stress, elastic modulus, and Poisson's ratio

The variation law of the peak deviatoric stress  $(\sigma_1 - \sigma_3)_p$  of HBPRC with respect to the confining pressure is shown in Fig. 6a. Because the confining pressure provides an interstitial pressure, the formation of defects in the HBPRC is constrained, increasing the peak deviatoric stress of the HBPRC. Additionally, under the uniaxial load, the improvement effect of the BF and PF on the peak deviatoric stress of concrete is very limited, and the peak deviatoric stresses are similar for BC-0.1, PC-0.1, BPC-0.1, and NC. Because



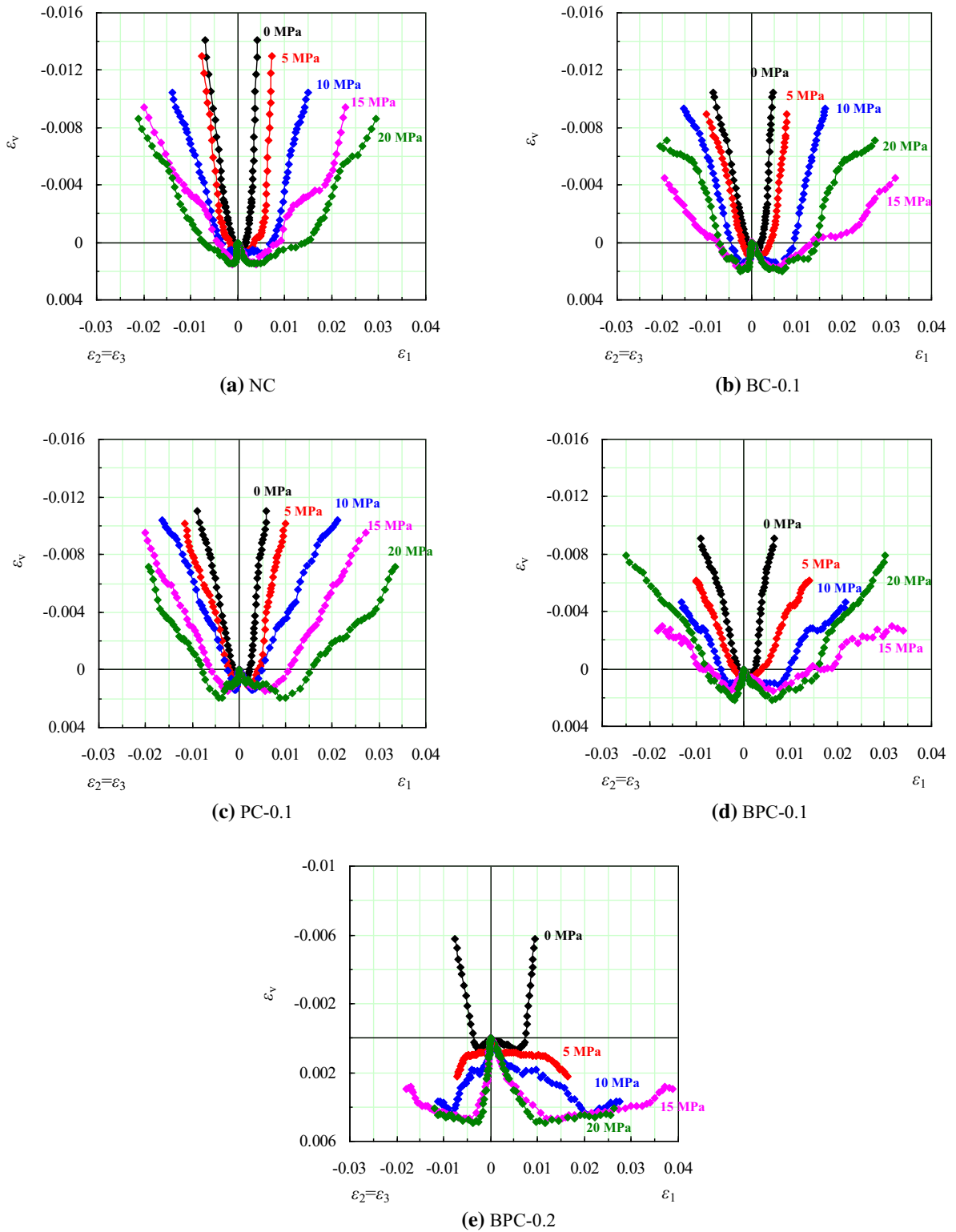
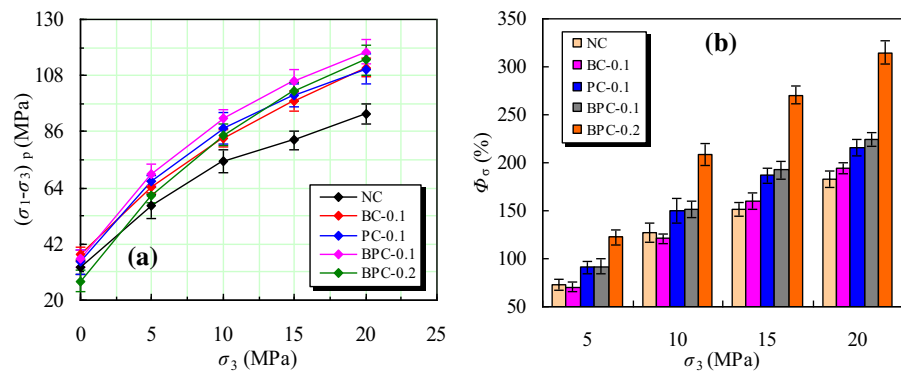


**Fig. 5** Variation of volumetric strain with axial and lateral strain of HBPRC at different confining pressures

**Fig. 6** Variation of **a** peak deviatoric stress and **b** increasing amplitude index of peak deviatoric stress with confining pressures



of the excessive fibre content, the peak deviatoric stress of BPC-0.2 is lower than that of NC. However, with an increase in the confining pressure, the differences between the peak deviatoric stress of NC and those of the other concretes gradually increase. When the confining pressure is 20 MPa, the peak deviatoric stress of BPC-0.2 is significantly higher than that of NC. Thus, the addition of BF and PF improves the confining pressure effect of the peak deviatoric stress. In this study, the increasing amplitude index is used to characterise the confining pressure effect of the peak deviatoric stress, that is

$$\Phi_\sigma = \frac{(\sigma_1 - \sigma_3)_p - \sigma_{1u}}{\sigma_{1u}} \quad (1)$$

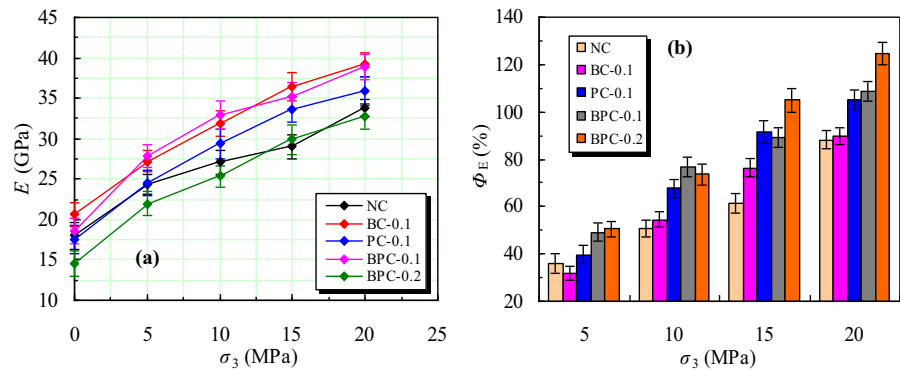
where  $\Phi_\sigma$  represents the increasing amplitude index of the peak deviatoric stress, and  $\sigma_{1u}$  represents the peak stress of HBPRC under uniaxial loading.

The variation of the increasing amplitude index of the peak deviatoric stress with respect to the confining pressure is shown in Fig. 6b. The addition of BF and PF significantly improves the confining pressure effect of the peak deviatoric stress of concrete. According to the fibre spacing theory [58], when a crack propagates to the interface between the fibres and the concrete matrix, shear stress that restrains the crack propagation is formed at the interface; consequently, the crack tends to close. At this time, the degree of stress concentration at the crack tip is reduced, and the crack development is restrained. However, under the confining pressure, because the localised macrocrack damage of HBPRC is restrained, the HBPRC gradually changes into ductile failure with multiple cracks. At this time, the crack-inhibition effect of the fibres is easier to be implemented, improving the confining pressure effect of the peak deviatoric stress of

concrete. Compared with BF, the hydrophobicity of PF leads to poor bonding between the PF and the concrete matrix [59], and the elastic modulus of PF is low. Therefore, the uniaxial strength of PC-0.1 is lower than that of BC-0.1. The confining pressure is more conducive to increasing the peak deviatoric stress for PC-0.1 than for BC-0.1; thus, the confining pressure effect of the peak deviatoric stress is greater for PC-0.1 than for BC-0.1. When BF and PF are mixed, the synergistic effects of the BF and PF are more conducive to crack inhibition; thus, the confining pressure effect of the peak deviatoric stress of BPC-0.1 is greater than that of BC-0.1 and PC-0.1. For BPC-0.2, the internal defects formed by excessive fibres lead to a more obvious improvement effect of the confining pressure on the peak deviatoric stress. Additionally, with an increase in the confining pressure, the amount of internal defects decreases, and the bonding performance between the fibres and the concrete matrix is enhanced. Moreover, the crack-inhibition effect of the BF and PF begins to be exerted. For the aforementioned two reasons, the peak deviatoric stress of BPC-0.2 exhibits the maximum confining pressure effect.

The elastic modulus  $E$  of HBPRC is defined as the slope of the straight line between 10 and 40% of the peak deviatoric stress in the longitudinal stress–strain curve. Its variation with respect to the confining pressure is shown in Fig. 7a. The change rule of the elastic modulus for HBPRC with respect to the confining pressure is consistent with that of the peak deviatoric stress. Owing to the constraint effect of the confining pressure on the initial defects in the concrete, the elastic modulus of HBPRC increases with the confining pressure, but the increasing trend gradually decreases. Furthermore, the addition of BF

**Fig. 7** Variation of **a** elastic modulus and **b** increasing amplitude index of elastic modulus with confining pressures



and PF improves the increasing amplitude of the elastic modulus with the increasing confining pressure. In this study, the confining pressure effect of the elastic modulus of HBPRC is characterised by the increasing amplitude index:

$$\Phi_E = \frac{E_p - E_u}{E_u} \quad (2)$$

where  $\Phi_E$  represents the increasing amplitude index of the elastic modulus, and  $E_p$  and  $E_u$  represent the elastic moduli of the HBPRC under the confining pressure and uniaxial loading, respectively. The variation of the increasing amplitude index of the elastic modulus with respect to the confining pressure is shown in Fig. 7b. Although the change law of the increasing amplitude index of the elastic modulus is slightly discrete, the overall change trend is similar to that for the increasing amplitude index of the peak deviatoric stress.

Theoretically, the elastic modulus represents the deformation resistance of material in the initial undamaged stage. In this stage, the crack-inhibition effect of the fibre is not exerted. In fact, because of the shrinkage, there is already initial damage, e.g. contraction cracks, in the concrete under the initial no-load condition. The addition of fibres can reduce the degree of concrete contraction, thus reducing the amount of contraction cracks in the concrete [60, 61]. However, for PC-0.1, the elastic modulus of PF is relatively low, and the bonding between the PF and the concrete matrix is relatively poor. Therefore, under a low confining pressure, the elastic modulus of PC-0.1 is slightly lower than that of NC. However, owing to the excessive BF and PF content, the elastic modulus of BPC-0.2 is significantly lower than that of NC under the low confining pressure. Furthermore, with the addition of BF and PF, the amount of interface

between the fibres and the concrete matrix increases, and the confinement effect of the confining pressure is more conducive to the improvement of the elastic modulus, thus increasing the confining pressure effect of the elastic modulus.

The Poisson's ratio of the HBPRC is defined as the ratio of the lateral strain to the longitudinal strain in the elastic deformation stage. Its variation with respect to the confining pressure is shown in Fig. 8. In general, the Poisson's ratio of the HBPRC decreases with the increasing confining pressure and gradually increases with the addition of BF and PF. Farnam et al. [35] studied the triaxial mechanical properties of slurry-infiltrated steel fibre concrete and reported that the Poisson's ratio of concrete increases with the steel fibre content and decreases with an increase in the confining pressure. The variation of the Poisson's ratio is generally consistent between slurry-infiltrated steel fibre concrete and HBPRC.

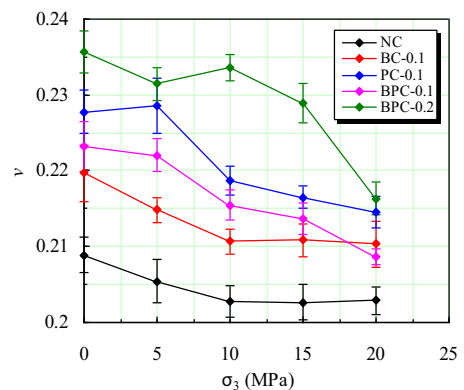


**Fig. 8** Variation of Poisson's ratio with confining pressures

### 3.3.2 Failure mode

The failure modes of HBPRC under different confining pressures are shown in Fig. 9. Under the uniaxial load, there are obvious longitudinal splitting cracks on the surface of NC after failure, and obvious fragment spalling occurs at the corner of the specimen, indicating typical brittle failure characteristics. Then, NC is further split along the longitudinal direction. It is found that the aggregate in NC is relatively intact, and the cracks mainly propagate along the interface transition zone between the aggregate and the concrete matrix. The cracks are relatively wide. Compared with NC, the integrity of the destroyed BPC-0.1 specimen under uniaxial loading is better, the fragment spalling

at the corner of the specimen is less obvious, and fine cracks are formed on the surface. BPC-0.1 is further split along the longitudinal direction. It is found that this specimen has more cracks than NC, but the cracks are relatively fine. The cracks mainly propagate along the interface transition zone between the aggregate and the concrete matrix. Compared with NC, the ductile failure characteristics of BPC-0.1 under uniaxial loading is more obvious. The bridging effect of the BF and PF limits the propagation of the single crack. The fine cracks are formed in the concrete to dissipate the energy generated by the load. Therefore, BPC-0.1 has more uniform damage development than NC, tends to undergo the overall large deformation failure, and exhibits obvious ductility characteristics.

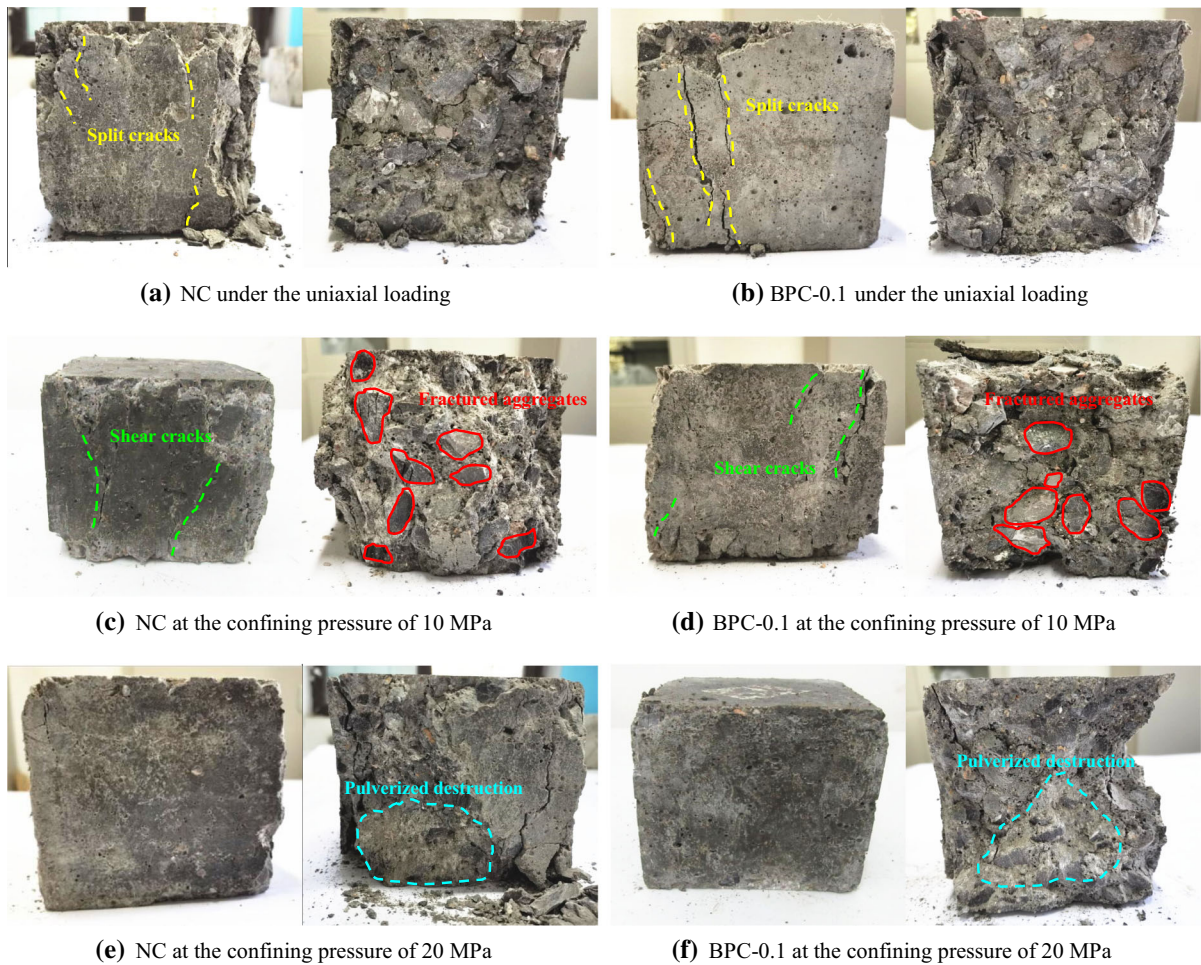


**Fig. 9** Failure mode of HBPRC at different confining pressures **a** NC under the uniaxial loading **b** BPC-0.1 under the uniaxial loading **c** NC at the confining pressure of 10 MPa **d** BPC-0.1 at

the confining pressure of 10 MPa **e** NC at the confining pressure of 20 MPa **f** BPC-0.1 at the confining pressure of 20 MPa



When the confining pressure increases to 10 MPa, several oblique shear cracks are formed on the surfaces of NC and BPC-0.1, indicating shear failure characteristics. Only a small number of fragments peel off at the corners of specimens. Compared with NC, BPC-0.1 has better integrity after failure. After the splitting of the NC and BPC-0.1 specimens, it is found that some aggregates in the specimens have been broken, indicating that the confining pressure restrains the formation of initial defects in the concrete, so that the cracks propagate through the aggregate. When the confining pressure increases to 20 MPa, there are no obvious cracks on the surface of NC and BPC-0.1, and only some extrusion failure characteristics are observed at the edges and corners of the specimens, indicating that the concrete specimens undergo extrusion plastic flow failure under the high confining pressure. There is no significant difference in integrity between the NC and BPC-0.1 specimens. After the splitting of the specimens, it is found that there are obvious fractures and dislocations in some areas of NC and BPC-0.1, indicating the failure characteristics of fragmentation. This confirms the extrusion plastic flow deformation of the concrete under the high confining pressure. Compared with the failure mode under uniaxial load, NC gradually exhibits ductile failure characteristics because of the confining pressure. The confining pressure can also restrain the development of localised damage in concrete, which makes the damage development of concrete more uniform when the concrete is destroyed and gradually leads to ductile failure characteristics. Therefore, with an increase in the confining pressure, the ductile failure characteristics of NC and BPC-0.1 gradually increase, while the difference between them gradually decreases, which is consistent with the analysis presented in Sect. 3.2.1.

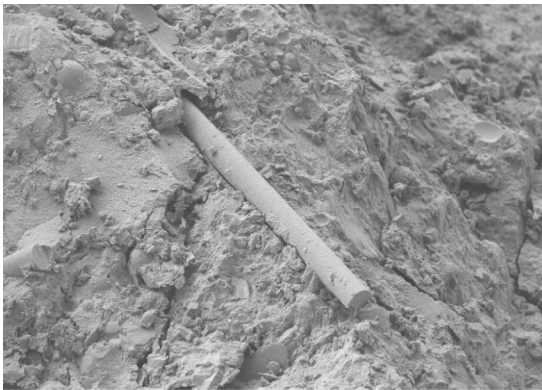
### 3.4 Action mechanism of BF and PF

The failure morphologies of the BF and PF under different confining pressures are shown in Fig. 10. Under the uniaxial load, the pull-out length of BF is large, and the surface of BF is smooth. However, under the confining pressure of 20 MPa, the BF is almost completely embedded in the concrete matrix, and its pull-out length is small. Bending fracture of the BF occurs, and the amount of hydration products on the surface of BF increases. Therefore, the increase in the

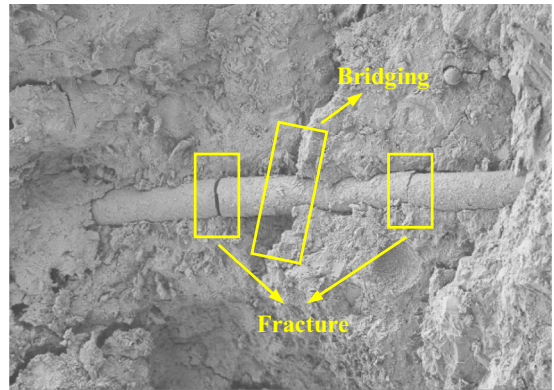
confining pressure improves the slipping resistance of BF, which not only enhances the triaxial strength of BC-0.1 but causes BC-0.1 to have a greater confining pressure effect than NC, as mentioned in Sect. 3.3.1.

As indicated by the cutting tip produced during fibre preparation, under the uniaxial load, the PF undergoes mainly pull-out failure, and its surface is relatively smooth, without obvious damage. When the confining pressure increases to 20 MPa, the pull-out length of PF decreases, and the PF exhibits obvious signs of tensile fracture. There are obvious scratches on the surface of PF, and the PF exhibits significant extrusion damage and torsion deformation. Therefore, the increase in the confining pressure increases the slipping resistance of PF, which not only increases the triaxial strength of PC-0.1 but also makes the confining pressure effect of PC-0.1 greater than that of NC. When BF and PF are mixed at the appropriate content, their synergistic effects improve the confining pressure effect on the mechanical properties of concrete. However, as shown in Fig. 10e, when the content of hybrid BF and PF is excessive, the dispersion uniformity of the BF and PF is reduced; thus, more bubbles are introduced in the mixing process, and the bonding performance between the fibres and the concrete matrix is degraded. Thus, the uniaxial strength of BPC-0.2 is low. However, with an increase in the confining pressure, the constraint effect of the confining pressure on the initial defects not only improves the triaxial strength of BPC-0.2 but also helps the BF and PF to restrain cracks; thus, the confining pressure effect of the triaxial mechanical properties of BPC-0.2 is improved.

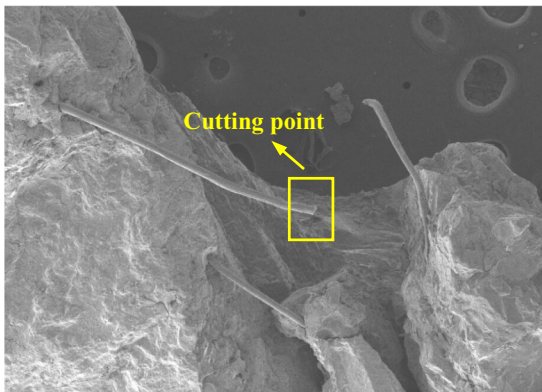
As indicated by Figs. 10a–d, the PF has a greater pull-out length than the BF under uniaxial and triaxial loading, indicating that the bonding performance between the BF and the concrete matrix is higher than that between the PF and the concrete matrix. Furthermore, because of the high elastic modulus, the BF is more conducive to inhibiting the initiation and propagation of cracks in the concrete. Therefore, the BF is mainly responsible for improving the strength of concrete. The bonding performance between the PF and the concrete matrix is relatively weak, and the PF has good ductility. Therefore, when the cracks propagate, the pull-out failure and the torsion and extrusion deformation of PF can effectively improve the deformation performance of concrete. Hence, compared



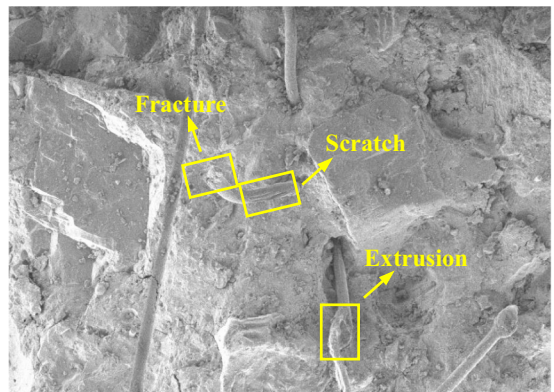
(a) Failure pattern of BF under uniaxial loading



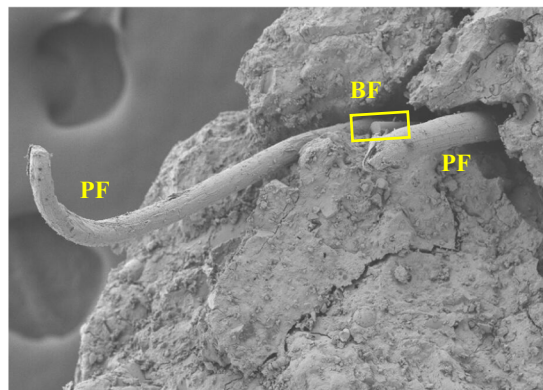
(b) Failure pattern of BF at the confining pressure of 20MPa



(c) Failure pattern of PF under uniaxial loading



(d) Failure pattern of PF at the confining pressure of 20MPa



(e) Distribution pattern of hybrid BF and PF in BPC-0.2

**Fig. 10** Failure morphology of BF and PF in HBPRC under different confining pressures **a** Failure pattern of BF under uniaxial loading **b** Failure pattern of BF at the confining pressure

of 20Mpa **c** Failure pattern of PF under uniaxial loading **d** Failure pattern of PF at the confining pressure of 20Mpa **e** Distribution pattern of hybrid BF and PF in BPC-0.2



with BF, the PF is more beneficial for improving the deformation performance of concrete.

#### 4 Strength criterion accounting for fibre effect

For quasi-brittle materials such as concrete and rock, scholars have established a variety of strength criteria based on mechanical theory or empirical analysis. Because of its small number of parameters and high calculation accuracy, the M–C strength criterion remains the most widely used strength criterion [62]. Its calculation formulas for the shear stress and maximum principal stress are as follows:

$$\tau = c + \sigma_n \tan \varphi \quad (3a)$$

$$\sigma_1 = 2c \frac{\cos \varphi}{1 - \sin \varphi} + \frac{1 + \sin \varphi}{1 - \sin \varphi} \sigma_3 \quad (3b)$$

where  $\tau$  represents the shear strength (in MPa),  $c$  represents the cohesive force (in MPa),  $\varphi$  represents the internal friction angle (in rad), and  $\sigma_n$  represents the normal stress acting on the shear plane (in MPa).

The M–C strength criterion has two limitations. First, the M–C strength criterion ignores the effect of the intermediate principal stress on the strength of materials. Second, the M–C strength criterion is a linear criterion for  $\sigma_1$  and  $\sigma_3$ . For concrete materials, the maximum principal stress does not always increase linearly with the increasing confining pressure [37, 38, 46, 47]. This is confirmed by the variation of the peak deviatoric stress of HBPRC with respect to the confining pressure (Sect. 3.3.1). In general, the cohesive force and internal friction angle of quasi-brittle materials change with changes in the confining pressure [62]. Therefore, in this study, Eqs. 4(a) and (b) are used to modify the cohesive force and internal friction angle of HBPRC to establish the nonlinear strength criterion for HBPRC.

$$c = c_0 + \Delta c \ln \left( \frac{\sigma_3}{P_a} \right) \quad (4a)$$

$$\varphi = \varphi_0 + \Delta \varphi \ln \left( \frac{\sigma_3}{P_a} \right) \quad (4b)$$

where,  $c_0$  and  $\varphi_0$  represent the cohesive force and internal friction angle of HBPRC under uniaxial loading, respectively;  $\Delta c$  and  $\Delta \varphi$  are the material

parameters related to the cohesive force and internal friction angle, respectively; and  $P_a = 0.10133$  MPa represents the standard atmospheric pressure.

For concrete materials, the cohesive force is mainly related to the amount of water and cementitious material; i.e. it is mainly related to the concrete strength. As indicated by the analysis presented in Sect. 3.3, the strength of HBPRC is influenced by the fibres. Therefore, there are correlations between the cohesive force of HBPRC and the fibre content. For ordinary concrete, the internal friction angle is mainly related to the contents of coarse and fine aggregates. For HBPRC, the crack bridging effect of fibres affects the crack propagation mode, thus affecting the failure mode of concrete. Therefore, for HBPRC with the same matrix component, the internal friction angle is mainly related to the fibre content.

By combining Eqs. 3b, 4a and b, the values of  $c_0$ ,  $\Delta c$ ,  $\varphi_0$ , and  $\Delta \varphi$  can be obtained via the regression fitting of  $\sigma_1$  and  $\sigma_3$  of HBPRC obtained in this study, and the fitted values of  $c_0$ ,  $\Delta c$ ,  $\varphi_0$ , and  $\Delta \varphi$  are listed in Table 2. Because both cohesive force and internal friction angle of HBPRC are influenced by the fibre content, by analysing the variation in the fitted values of  $c_0$ ,  $\Delta c$ ,  $\varphi_0$ , and  $\Delta \varphi$  with the fibre content, the relationships between the parameters ( $c_0$ ,  $\Delta c$ ,  $\varphi_0$ ,  $\Delta \varphi$ ) and the fibre content can be represented by the following formulas:

$$c_0 = a_1 + b_1 V_1 + c_1 V_1 V_2 + d_1 V_1^2 \quad (5a)$$

$$\Delta c = a_2 + b_2 V_1 + c_2 V_1^2 + d_2 V_2^2 \quad (5b)$$

$$\varphi_0 = 0.06 \exp(a_3 V_1 + b_3 V_2 + c_3 V_1^2) + d_3 \quad (5c)$$

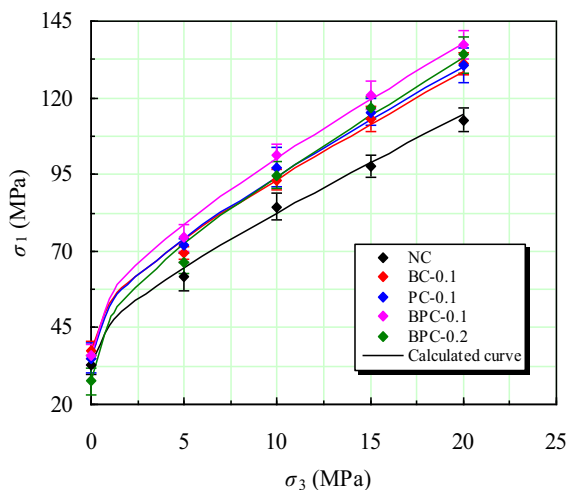
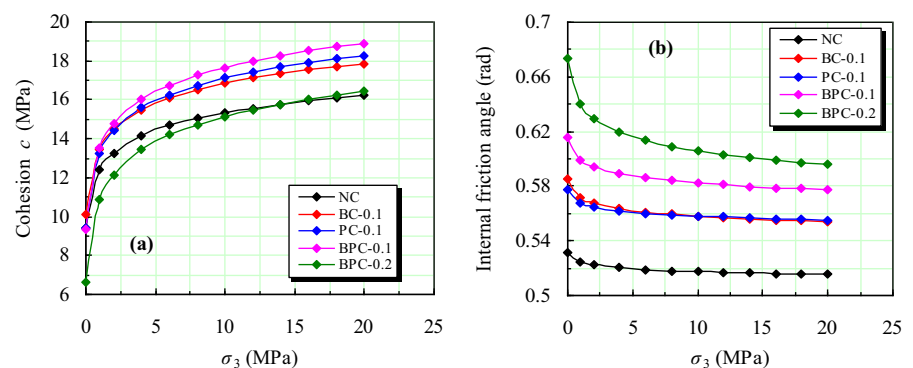
$$\Delta \varphi = -0.003 \exp(a_4 V_1 + b_4 V_2 + c_4 V_1 V_2 + d_4 V_1^2) \quad (5d)$$

where  $V_1$  and  $V_2$  represent the volume contents of BF and PF, respectively (in vol.%), and  $a_1$ – $a_4$ ,  $b_1$ – $b_4$ ,  $c_1$ – $c_4$ , and  $d_1$ – $d_4$  are fitting coefficients. The fitted results are presented in Table 2.

The variations of the cohesive force and internal friction angle of HBPRC with respect to the confining pressure are calculated using Eqs. 5a–d and are presented in Fig. 11. With the increasing confining pressure, the cohesive force of HBPRC increases and the internal friction angle decreases, which is consistent with the variation reflected by the stress Mohr

**Table 2** The fitted values of parameters in Eqs. (4a), (4b), (5a) ~ (5d)

Parameter	$c_0$	$\Delta c$	$\varphi_0$	$\Delta \varphi$				
NC	9.4497	1.2636	0.5311	- 0.0030				
BC-0.1	10.0229	1.4514	0.5858	- 0.0060				
PC-0.1	9.4543	1.6914	0.5772	- 0.0042				
BPC-0.1	9.4298	1.8108	0.6158	- 0.0073				
BPC-0.2	6.6057	1.8684	0.6738	- 0.0148				
Coefficients	$a_1$	9.4367	$a_2$	1.2856	$a_3$	17.3282	$a_4$	16.3173
	$b_1$	25.1792	$b_2$	15.1942	$b_3$	5.6992	$b_4$	3.2450
	$c_1$	- 348.135	$c_2$	- 133.703	$c_3$	- 108.5329	$c_4$	57.2708
	$d_1$	- 185.083	$d_2$	38.5360	$d_3$	0.4711	$d_4$	- 93.3595

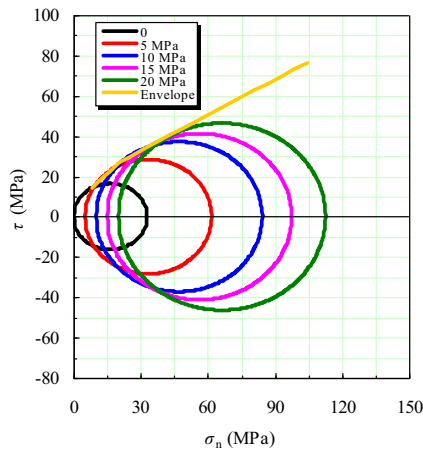
**Fig. 11** Variation of **a** cohesion and **b** internal friction angle of HBPRC with confining pressure**Fig. 12** Comparison between the calculated results of the proposed strength criterion and the experimental results

circle and the strength envelope of quasi-brittle materials such as rock and concrete [62].

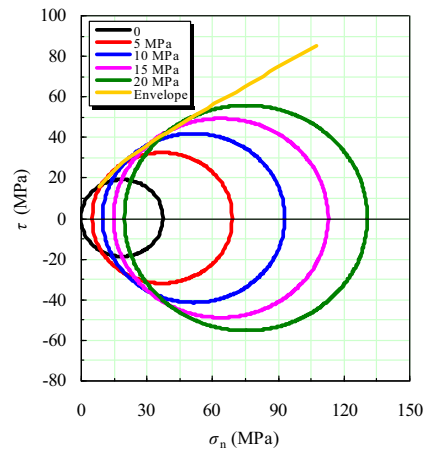
The nonlinear M–C strength criterion for HBPRC is established by combining Eqs. 3b, 4a and b, and 5a–d. Figure 12 shows a comparison between the calculated

values of the proposed nonlinear M–C strength criterion and the experimental results for HBPRC. The calculated results of the nonlinear M–C strength criterion agree well with the experimental results. The nonlinear M–C strength criterion accurately reflects not only the nonlinear variation of the strength of HBPRC with respect to the confining pressure but also the effects of the types of fibres added on the triaxial strength of HBPRC. The relationship between the Mohr's circle of stress and the strength envelope curve of the HBPRC calculated using the established nonlinear M–C strength criterion is shown in Fig. 13. The strength envelope of the HBPRC is essentially tangent to each Mohr's circle of stress, indicating the applicability of the proposed nonlinear M–C strength criterion for the characterisation of the triaxial strength of HBPRC. However, as shown in Fig. 13, the nonlinear characteristics of the strength envelope of HBPRC are not obvious, which is attributed to the low confining pressure in this study. Therefore, the triaxial mechanical properties of HBPRC under high confining pressures ( $> 20$  MPa) should be investigated. Accordingly, the established

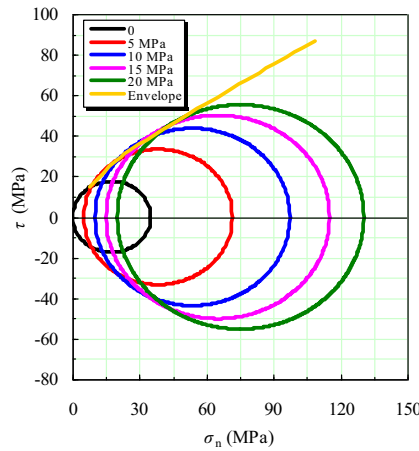
**Fig. 13** Mohr circles and strength envelopes of HBPRC **a** NC **b** BC-0.1 **c** PC-0.1 **d** BPC-0.1 **e** BPC-0.2



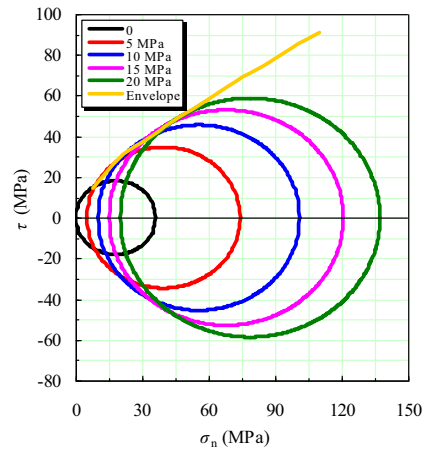
**(a)** NC



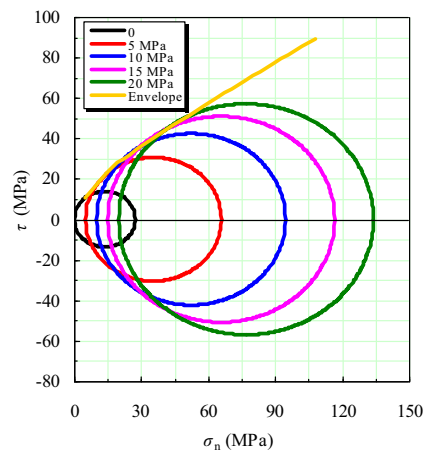
**(b)** BC-0.1



**(c)** PC-0.1



**(d)** BPC-0.1



**(e)** BPC-0.2

nonlinear M–C strength criterion can be modified to widen its application scope.

## 5 Conclusions

The triaxial mechanical properties of HBPRC were investigated, and the hydrostatic behaviour, deviatoric behaviour, and confining pressure effect of the limit state were analysed. The action mechanism of BF and PF was revealed. Finally, a nonlinear M–C strength criterion for HBPRC was established. The following conclusions are drawn.

(1) The  $\sigma_m$ - $\varepsilon_v$  curves of NC, BC-0.1, PC-0.1, and BPC-0.1 exhibit a two-stage change characteristic, whereas the  $\sigma_m$ - $\varepsilon_v$  curve of BPC-0.2 exhibits an obvious three-stage change characteristic.

(2) The confining pressure increases the ductile deformation of HBPRC. The addition of BF and PF increases the deformation and ductility of concrete, but an increase in the confining pressure weakens the effects of BF and PF on the ductility of concrete. With the increasing confining pressure and the fibre addition, the volume contraction strain of HBPRC increases, but the volume expansion strain decreases.

(3) The peak deviatoric stress and elastic modulus of HBPRC increase nonlinearly with the increasing confining pressure. The fibre addition increases the Poisson's ratio of concrete, while the confining pressure reduces the Poisson's ratio. With the increasing confining pressure, the failure mode of HBPRC gradually changes from longitudinal split failure to oblique shear failure and extrusion plastic flow failure.

(4) The confining pressure increases the slipping resistance of BF and PF, resulting in severe damage to BF and PF when they are pulled out. BF is mainly responsible for improving the strength of concrete, and PF is more conducive to improving the deformation performance.

(5) A nonlinear M–C strength criterion for HBPRC is established. The calculation results of the nonlinear M–C strength criterion agree well with the experimental results, and the strength envelope is essentially tangent to the Mohr's circle of stress, which verifies the rationality of the established nonlinear M–C strength criterion.

In the study, the triaxial mechanical properties of HBPRC with only one matrix strength grade of C30 were investigated. Different sizes of fibres can

influence the mechanical properties of concrete at different scale levels, and the same type of fibres or the same combination mode of hybrid fibres have different influence on the mechanical properties of concrete with different qualities. Therefore, further systematic study on the influence of different combination modes of hybrid fibres, especially the hybrid macro-fibres and micro-fibres, on the triaxial mechanical properties of concrete with different qualities will be more helpful to improve the effective utilization of fibres in concrete.

**Funding** This study was funded by the National Natural Science Foundation of China (Grant No. 51590914, 51608432), Natural Science Foundation of Shaanxi Province (Grant No. 2019JQ-481).

## Declarations

**Conflict of interest** The authors declare that they have no conflict of interest.

**Open Access** This article is licensed under a Creative Commons Attribution 4.0 International License, which permits use, sharing, adaptation, distribution and reproduction in any medium or format, as long as you give appropriate credit to the original author(s) and the source, provide a link to the Creative Commons licence, and indicate if changes were made. The images or other third party material in this article are included in the article's Creative Commons licence, unless indicated otherwise in a credit line to the material. If material is not included in the article's Creative Commons licence and your intended use is not permitted by statutory regulation or exceeds the permitted use, you will need to obtain permission directly from the copyright holder. To view a copy of this licence, visit <http://creativecommons.org/licenses/by/4.0/>.

## References

- Walton PL, Majumdar AJ (1975) Cement-based composites with mixtures of different types of fibres. *Compos* 6(5):209–216
- Ruiz G, de la Rosa Á, Poveda E (2019) Relationship between residual flexural strength and compression strength in steel-fiber reinforced concrete within the new Eurocode 2 regulatory framework. *Theor Appl Fract Mech* 103:102310
- Yoo DY, Banthia N (2019) Impact resistance of fiber-reinforced concrete—A review. *Cem Concr Compos* 104:103389
- Niu D, Li D, Fu Q (2020) A 3D-IFU model for characterizing the pore structure of hybrid fibre-reinforced concrete. *Mater Des* 188:108473
- Çelik Z, Bingöl AF (2020) Fracture properties and impact resistance of self-compacting fiber reinforced concrete (SCFRC). *Mater Struct* 53:50–65



6. Ruiz G, de la Rosa Á, Wolf S, Poveda E (2018) Model for the compressive stress-strain relationship of steel fiber-reinforced concrete for non-linear structural analysis. *Hormigón y Acero* 69(S1):75–80
7. de la Rosa Á, Ruiz G, Poveda E (2019) Study of the compression behavior of steel-fiber reinforced concrete by means of the response surface methodology. *Appl Sci* 9(24):5330
8. Dong S, Han B, Yu X, Ou J (2019) Constitutive model and reinforcement mechanisms of uniaxial compressive property for reactive powder concrete with super-fine stainless wire. *Compos Part B Eng* 166:298–309
9. Chi Y, Xu LH, Zhang YY (2014) Experimental study on hybrid fiber-reinforced concrete subjected to uniaxial compression. *J Mater Civ Eng* 26(2):211–218
10. Ralegaonkar R, Gavali H, Aswath P, Abolmaali S (2018) Application of chopped basalt fibers in reinforced mortar: a review. *Constr Build Mater* 164:589–602
11. Rybin VA, Utkin AV, Baklanova NI (2013) Alkali resistance, microstructural and mechanical performance of zirconia-coated basalt fibers. *Cem Concr Res* 53:1–8
12. Buendía AML, Sánchez MDR, Climent V, Guillem C (2013) Surface treated polypropylene (PP) fibres for reinforced concrete. *Cem Concr Res* 54:29–35
13. Qian CX, Stroeven P (2000) Development of hybrid polypropylene-steel fibre-reinforced concrete. *Cem Concr Res* 30(1):63–69
14. Branston J, Das S, Kenno SY, Taylor C (2016) Mechanical behaviour of basalt fibre reinforced concrete. *Constr Build Mater* 124:878–886
15. Sun X, Gao Z, Cao P, Zhou C (2019) Mechanical properties tests and multiscale numerical simulations for basalt fiber reinforced concrete. *Constr Build Mater* 202:58–72
16. Dilbas H, Çakir Ö (2020) Influence of basalt fiber on physical and mechanical properties of treated recycled aggregate concrete. *Constr Build Mater* 254:119216
17. Li M, Gong F, Wu Z (2020) Study on mechanical properties of alkali-resistant basalt fiber reinforced concrete. *Constr Build Mater* 245:118424
18. Wang Y, Li S, Peter H, Fan Y (2020) Mechanical properties and microstructure of basalt fibre and nano-silica reinforced recycled concrete after exposure to elevated temperatures. *Constr Build Mater* 247:118561
19. Jiang C, Fan K, Wu F, Chen D (2014) Experimental study on the mechanical properties and microstructure of chopped basalt fibre reinforced concrete. *Mater Des* 58:187–193
20. Asprone D, Cadoni E, Lucolano F, Prota A (2014) Analysis of the strain-rate behavior of a basalt fiber reinforced natural hydraulic mortar. *Cem Concr Compos* 53:52–58
21. Altalabani D, Bzeni DKH, Linsel S (2020) Mechanical properties and load deflection relationship of polypropylene fiber reinforced self-compacting lightweight concrete. *Constr Build Mater* 252:119084
22. Qin Y, Zhang X, Chai J, Xu Z, Li S (2019) Experimental study of compressive behavior of polypropylene-fiber-reinforced and polypropylene-fiber-fabric-reinforced concrete. *Constr Build Mater* 194:216–225
23. Karimipour A, Ghalehnavi M, Brito J, Attari M (2020) The effect of polypropylene fibres on the compressive strength, impact and heat resistance of self-compacting concrete. *Struct* 25:72–87
24. Song PS, Hwang S, Sheu BC (2005) Strength properties of nylon-and polypropylene-fiber-reinforced concretes. *Cem Concr Res* 35(8):1546–1550
25. Alhozaimy AM, Soroushian P, Mirza F (1996) Mechanical properties of polypropylene fiber reinforced concrete and the effects of pozzolanic materials. *Cem Concr Compos* 18(2):85–92
26. Li ZX, Li CH, Shi YD, Zhou XJ (2017) Experimental investigation on mechanical properties of hybrid fibre reinforced concrete. *Constr Build Mater* 157:930–942
27. Smarzewski P (2019) Influence of basalt-polypropylene fibres on fracture properties of high performance concrete. *Compos Struct* 209:23–33
28. Wang D, Ju Y, Shen H, Xu L (2019) Mechanical properties of high performance concrete reinforced with basalt fiber and polypropylene fiber. *Constr Build Mater* 197:464–473
29. Zhang H, Wang L, Bai L, Addae M, Neupane A (2019) Research on the impact response and model of hybrid basalt-macro synthetic polypropylene fiber reinforced concrete. *Constr Build Mater* 204:303–316
30. Fu Q, Xu W, Li D, Li N, Niu D, Zhang L, Guo B, Zhang Y (2021) Dynamic compressive behaviour of hybrid basalt-polypropylene fibre-reinforced concrete under confining pressure: experimental characterisation and strength criterion. *Cem Concr Compos* 118:103954
31. Richart FE, Brantzaeg A, Brown RL (1929) The failure of plain and spirally reinforced columns in compression. *Uni Illinois Eng Exp Sta Bull* 190:120
32. Khan MZN, Hao Y, Hao H, Shaikh FUA, Liu K (2018) Mechanical properties of ambient cured high-strength plain and hybrid fiber reinforced geopolymer composites from triaxial compressive tests. *Constr Build Mater* 185:338–353
33. Zeng S, Ren X, Li J (2013) Triaxial behavior of concrete subjected to dynamic compression. *J Struct Eng* 139(9):1582–1592
34. He Z, Song Y (2010) Triaxial strength and failure criterion of plain high-strength and high-performance concrete before and after high temperatures. *Cem Concr Res* 40(1):171–178
35. Farnam Y, Moosavi M, Shekarchi M, Babanajad SK, Bagherzadeh A (2010) Behaviour of slurry infiltrated fibre concrete (SIFCON) under triaxial compression. *Cem Concr Res* 40(11):1571–1581
36. Hammoud R, Yahia A, Boukhili R (2014) Triaxial compressive strength of concrete subjected to high temperature. *J Mater Civ Eng* 26(4):705–712
37. Chen D, Yu X, Liu R, Li S, Zhang Y (2019) Triaxial mechanical behavior of early age concrete: experimental and modelling research. *Cem Concr Res* 115:433–444
38. Chen D, Yu X, Shen J, Liao Y, Zhang Y (2017) Investigation of the curing time on the mechanical behavior of normal concrete under triaxial compression. *Constr Build Mater* 147:488–496
39. Lu X, Hsu CTT (2007) Stress-strain relations of high-strength concrete under triaxial compression. *J Mater Civ Eng* 19(3):261–268
40. Chen Z, Hu Y, Li Q, Sun M, Lu P, Liu T (2010) Behavior of concrete in water subjected to dynamic triaxial compression. *J Eng Mech* 136(3):379–390



41. Lu X, Hsu CTT (2006) Behavior of high strength concrete with and without steel fiber reinforcement in triaxial compression. *Cem Concr Res* 36(9):1679–1685
42. Lim JC, Ozbakkaloglu T (2014) Stress-strain model for normal- and light-weight concretes under uniaxial and triaxial compression. *Constr Build Mater* 71:492–509
43. Zhou W, Feng P, Lin H (2020) Constitutive relations of coral aggregate concrete under uniaxial and triaxial compression. *Constr Build Mater* 251:118957
44. Cusson D, Paultre P (1995) Stress-strain model for confined high-strength concrete. *J Struct Eng* 121(3):468–477
45. Imran I, Pantazopoulou S (1996) Experimental study of plain concrete under triaxial stress. *ACI Mater J* 93(6):589–601
46. Malecot Y, Zingg L, Briffaut M, Baroth J (2019) Influence of free water on concrete triaxial behavior: the effect of porosity. *Cem Concr Res* 120:207–216
47. Zingg L, Briffaut M, Baroth J, Malecot Y (2016) Influence of cement matrix porosity on the triaxial behaviour of concrete. *Cem Concr Res* 80:52–59
48. Vu XH, Malecot Y, Daudeville L, Buzaud E (2009) Experimental analysis of concrete behavior under high confinement: effect of the saturation ratio. *Int J Solids Struct* 46(5):1105–1120
49. Piotrowska E, Malecot Y, Ke Y (2014) Experimental investigation of the effect of coarse aggregate shape and composition on concrete triaxial behavior. *Mech Mater* 79:45–47
50. Song L, Huang SM, Yang SC (2004) Experimental investigation on criterion of three-dimensional mixed-mode fracture for concrete. *Cem Concr Res* 34(6):913–916
51. Dutra VFP, Maghous S, Filho AC (2013) A homogenization approach to macroscopic strength criterion of steel fiber reinforced concrete. *Cem Concr Res* 44:34–45
52. Vu XH, Malecot Y, Daudeville L, Buzaud E (2009) Effect of the water/cement ratio on concrete behavior under extreme loading. *Int J Numer Anal Methods Geomech* 33(17):1867–1888
53. Jiang H (2017) A failure criterion for rocks and concrete based on the Hoek-Brown criterion. *Int J Rock Mech Min Sci* 95:62–72
54. Shang H, Song Y (2008) Behavior of air-entrained concrete under the compression with constant confined stress after freeze-thaw cycles. *Cem Concr Compos* 30(9):854–860
55. Yu Z, Huang Q, Xie X, Xiao N (2018) Experimental study and failure criterion analysis of plain concrete under combined compression-shear stress. *Constr Build Mater* 179:198–206
56. Fu Q, Niu D, Zhang J, Huang D, Wang Y, Hong M, Zhang L (2018) Dynamic compressive mechanical behaviour and modelling of basalt-polypropylene fibre-reinforced concrete. *Arch Civ Mech Eng* 3(18):914–927
57. Xie SY, Shao JF, Burlion N (2008) Experimental study of mechanical behaviour of cement paste under compressive stress and chemical degradation. *Cem Concr Res* 38(12):1416–1423
58. Wu ZM, Shi CJ, He W, Wang DH (2017) Static and dynamic compressive properties of ultra-high performance concrete (UHPC) with hybrid steel fiber reinforcements. *Cem Concr Compos* 79:148–157
59. Ranjbar N, Talebian S, Mehrali M, Kuenzel C, Metselaar HSC, Jumaat MZ (2016) Mechanisms of interfacial bond in steel and polypropylene fiber reinforced geopolymer composites. *Compos Sci Technol* 122:73–81
60. Branston J, Das S, Kenno SY, Taylor C (2016) Influence of basalt fibres on free and restrained plastic shrinkage. *Cem Concr Compos* 74:182–190
61. Alrshoudi F, Mohammadhosseini H, Tahir MM, Alyousef R, Alghamdi H, Alharbi Y, Alsaif A (2020) Drying shrinkage and creep properties of prepacked aggregate concrete reinforced with waste polypropylene fibers. *J Build Eng* 26:101522
62. Singh M, Raj A, Singh B (2011) Modified Mohr-Coulomb criterion for non-linear triaxial and polyaxial strength of intact rocks. *Int. J Rock Mech Min Sci* 48(4):546–555

**Publisher's Note** Springer Nature remains neutral with regard to jurisdictional claims in published maps and institutional affiliations.

